# Algae pyrolysis in alkaline molten salt: Products transformation

Jun Li, Kuo Zeng, Dian Zhong, Xin Chen, Ange Nzihou, Haiping Yang, Hanping Chen

# Algae pyrolysis in alkaline molten salt: Products transformation

Jun Li [a], Kuo Zeng [a,], Dian Zhong [a], Xin Chen [a], Ange Nzihou [b], Haiping Yang [a], Hanping Chen [a]

[a] State Key Laboratory of Coal Combustion, Huazhong University of Science and Technology, 1037 Luoyu Road, Wuhan, Hubei 430074, PR China
[b] Universit´e de Toulouse, IMT Mines Albi, RAPSODEE CNRS UMR 5302, Campus Jarlard, F.81013 Albi Cedex 09, France

A B S T R A C T

Algae pyrolysis in alkaline molten salt is a promising technology for hydrogen production, but the pyrolysis products transformation has not clearly been described up-to-date. Moreover, the complex bio-oil especially heavy bio-oil fraction directly influences the products transformation pathways, while limiting the hydrogen production yield and application. Both the light and heavy bio-oil fractions are investigated in detail and the effect of alkaline molten salt on products transformation is obtained. Molten salt promotes the cyclization and aromatization of linear alkenes, thereby increasing aromatic compound content and hydrogen production. The decarbonation of $Na_2CO_3$ and the deoxygenation of NaOH lead to the methane release, in turn reducing hydrogen production. The heavy compounds tend to polymerize at higher temperatures into compounds with higher molecular weights and unsaturation, while generating hydrogen. As the temperature rises, char reacts with molten salt to form hydrogen and disappears at 650 °C, while aromatics in light compounds condense into heavy compounds, which then grow to form soot-like at 600 °C, accompanying hydrogen release. Based on the relationship between products transformation, hydrogen release and alkaline molten salt effect, strategies to improve the hydrogen yield and purity of AMSP process are proposed.

## 1. Introduction

Promoting clean and sustainable energy is of great significance for ensuring energy security and promoting environmental protection [1,2]. In recent years, biomass has been recognized as a prospective renewable energy source to address these challenges, among which algae is attracting increasing attention due to its fast growth rate, high photosynthetic efficiency and global distribution [3,4]. The production of biofuels such as bioethanol and biohydrogen is the foremost option when considering algae refining strategies [5,6]. For algae refining processes, thermochemical processes are favored over biochemical processes because of their advantages of high utilization rate, low cost and fast kinetics [7]. As hydrogen is a clean-renewable energy carrier with high energy density, many researchers have produced algae-based hydrogen using pyrolysis, gasification and liquefaction, but these methods are subject to high energy consumption, high operating pressure, salt precipitation and low hydrogen yield etc. [8–11].

Molten salt has been widely used as an excellent catalytic and heating medium for the thermochemical conversion of carbon-containing materials to accelerate the reaction rate and regulate the product composition [12,13]. It can also retain a certain amount of ash in algae to prevent slagging or salt precipitation at high temperature [8]. Recently, our group investigated the potential of algae pyrolysis in alkaline molten NaOH-$Na_2CO_3$ (referred to as AMSP, as shown in reaction (1) for hydrogen production and obtained a stable high hydrogen yield of 71.48 mmol/g-algae in continuous operation [8]. Algae not only act as a hydrogen source, but also as a source of carbon and water source (generated by algae pyrolysis [14]) to extract hydrogen from NaOH. More importantly, the $CO_X$ (CO and $CO_2$) product reacts with molten NaOH to form $Na_2CO_3$, significantly reducing the carbon footprint, and the used salt can be subsequently regenerated by industrial waste calcium carbide slag or used as valuable chemical in a wide range of applications [15]. Moreover, molten salt can be used to store solar heat and heat released from biomass decomposition for algae pyrolysis [16], saving the cost of energy consumption needed for heating.

$$C_1H_{1.69}O_{0.56}N_{0.14}S_{0.006} + aNaOH \rightarrow bNa_2CO_3 + cH_2 + salt + char + liquid + gas \quad (1)$$

Studies have shown that the effects of component interaction of bio-oil (light and heavy fraction) can affect the transformation and composition of pyrolysis products [17,18]. And the transformation of hydrogen-containing compounds further affects hydrogen production.

However, the pyrolysis products transformation (especially heavy bio-oil) during the AMSP process has not clearly been described up-to-date. Studies have explored the effect of molten alkaline salt (mostly carbonates) during the pyrolysis of carbon contained feedstock [19–21], but little research has been done on alkaline molten salt (hydroxides). Although both molten carbonates and molten hydroxides are basic and have similar alkali metal ions, they provide different effects during the pyrolysis. For example, hydroxides can serve as a hydrogen donor for hydrogen production and be used to destroy the original structure of biomass [8,22].

Typically, the heavy components constitute over 50 wt% of the total species in bio-oil [23,24]. However, the inherent properties of heavy components (molecular weight > 200 Da) together with high boiling points and complex structures make their investigation challenging [25,26]. Recently, the advanced Fourier transform ion cyclotron resonance mass spectrometer (FT-ICR-MS) equipped with electrospray ionization (ESI) has been successfully applied to identify the heavy bio-oil compounds derived from the pyrolysis of various biomass [19,27–29]. Consequently, the bio-oil transformation, especially heavy bio-oil fraction, during the AMSP process could be investigated in insight.

In this work, the experiments were conducted in the temperature range of 500–750 °C (thermal stabilization interval of alkaline molten salt) to study the products transformation with emphasis on hydrogen production [8]. A combination of GC–MS and FT-ICR-MS was used to identify the light and heavy bio-oil compounds in depth. Based on the detailed bio-oil composition, the transformation pathways of pyrolysis products as well as strategies to further improve hydrogen yield and purity were proposed.

## 2. Material and methods

### 2.1. Materials

Nannochloropsis sp. with particle size less than 0.6 mm was first dried at 105 °C for 24 h and then pressed in a cylindrical mold to produce pellets (0.23 ± 0.005 g) with a diameter of 6 mm and a height of 6.5 mm. The purpose of pelleting is to reduce transportation costs caused by the low volume and energy density of raw algae. The ultimate and proximate analysis results of feedstock were presented in Table S1. Details on chemical composition of algae, as well as the test methods of ultimate and proximate analysis can be found in detail in our previous studies [8,27]. Sodium carbonate and sodium hydroxide powder were bought from the Sinopharm Chemical Reagent Co., Ltd (Shanghai, China). The mixture of sodium hydroxide and sodium carbonate (mass ratio 8:2, with a melting point of approx. 289 °C) was not pre-melted for homogeneity, as it is strongly absorbent.

### 2.2. Experimental methods

The AMSP experiments of algae were carried out on the apparatus as shown in Fig. S1, which mainly comprises a graphite crucible (carbon content > 99.9, 250 mm height, 40 mm i.d. and 44 mm o.d.), an enclosure (Hastelloy C276, 70 mm i.d.), a feeding unit, an electric furnace with temperature control system and a volatile collection system. The graphite crucible acted as a reactor to contain the molten salt, and the feeding unit stored algae pellets, which were then fed through a feed tube (Hastelloy C276, 10 mm i.d.) into the molten salt for pyrolysis. $N_2$ was used to stir the molten salt through a bubble tube (Hastelloy C276, 1.7 mm i.d.) to obtain homogeneous molten salt similar to that achieved by pre-melting. The openings for the feed and bubble tubes were placed 15 mm and 8 mm above the bottom of molten salt, respectively, while the perforated plate was positioned 8–10 mm below the upper surface of the molten salt. It should be mentioned that the pore size of the perforated plate was changed from 1.2 mm (previous work [8]) to 0.5 mm for sufficient reaction of some small char particles. This optimized design resulted in some changes in product distribution and gas yield compared to previous work [8].

Prior to the AMSP experiment, $N_2$ (250 mL/min) was introduced through the feed tube for 30 min to exhaust the air in the enclosure. Another $N_2$ (200 mL/min) was introduced through the bubbling tube to stir the molten salt as soon as the temperature reaches 400 °C. After the target temperature (500 °C, 550 °C, 600 °C, 650 °C, 700 °C and 750 °C) was reached, ten algae pellets were fed into 110 g of molten NaOH-$Na_2CO_3$ to undergo pyrolysis, and the reaction lasted 25 min. Each experiment was performed 3 times. The liquid product containing bio-oil and water was condensed in the ice-water bath, the gases were collected by a sample bag (Dalian Delin Gas Packing Co., Ltd), and the remaining char in the crucible was soaked in deionized water, filtered and collected. The methods for calculating the yield of each product was described in a previous work [8]. In addition, Inconel series (Inconel 625) and Hastelloy-N (GH3535) are suggested to be used as the materials of reactor and pipelines to provide resistance to the corrosion of alkaline molten salt in industrial applications [30,31].

It should be noted that at temperatures above 550 °C, there was solid products formed in the ice-water bath, referred to as soot-like in this paper, and was also collected for subsequent analysis. In addition, for comparison, the pyrolysis experiments (SP) were performed on this apparatus under the same reaction temperatures. SPT and AMSPT are used to represent the experimental conditions, where T represents the reaction temperature.

### 2.3. Characterization

The gas products were analyzed by an off-line gas chromatography (Panna A91, China) equipped with a 5A molecular sieve column, a Porapak Q column and an $Al_2O_3$/KCl capillary column. CO, $H_2$, $CH_4$ and $CO_2$ were detected by a thermal conductivity detector, while olefins and alkanes ($C_{2+}$) were detected by a flame ionization detector. The columns were first maintained at 80 °C for 4 min, then heated to 150 °C at 10 °C/min, and finally held at 150 °C for 6 min.

The ultimate analysis of solid products and algae was measured using an CHN/O elemental analyzer (Vario Micro Cube, Germany). For char and soot-like, a field emission scanning electron microscopy (FE-SEM, ZEISS Gemini 300, Germany) was used to investigate the morphology, an X-ray diffraction spectroscopy (XRD, SmartLab-SE, Japan) with Cu Kα radiation at λ = 1.5406 Å was used to analyze the microcrystalline structure, and a Raman spectroscopy (inVia-Reflex, China) equipped with Nd-YAG laser (wavelength 532 nm) was employed to characterize the carbon skeleton with the spectrum integrated three times to improve the signal-to-noise ratio. For both XRD and Raman tests, each sample was tested three times in different zones to reflect the overall properties of solid products.

The liquid products were first dehydrated using anhydrous magnesium sulphate and tested by a gas chromatograph-mass spectrometer (GCMS, Agilent 7890 A series GC coupled with a 5975 MS detector) with a capillary column (HP-5MS, 30 m × 0.25 mm i.d. × 0.25 um d.f.). The detail settings of the GCMS were as follows: the injection temperature was 280 °C, the split ratio was 20:1, and the carrier gas in the column was set as 1 mL/min. The temperature in oven was first maintained at 40 °C (2 min), and then heated to 200 °C at 5 °C/ min (held for 5 min), and finally heated to 300 °C at 10 °C/ min (held for 5 min). All the compounds were identified using a National Institute of Standards and Technology Library (NIST 14.L).

The heavy components in the bio-oil were analyzed using a FT-ICR-MS (7.0 T Solarix, Germany) equipped with ESI in positive-ion mode. The bio-oil samples were first dehydrated with anhydrous magnesium sulfate and then diluted with methanol to 0.35 mg/ml. Before analysis, the bio-oil solution was spiked with 0.5 vol% of formic acid to enhance the ionization of organic compounds. The emitter voltage, capillary voltage and end plate offset were set as 4.0 kV, 4.5 kV and − 0.5 kV, respectively. The flight time was set as 0.5 ms and a total of 128 scans

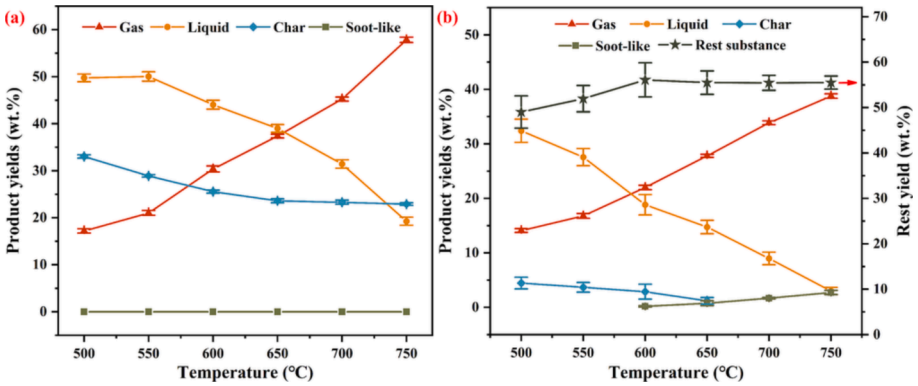


**Fig. 1.** Products distribution for: (a) SP and (b) AMSP at different temperatures.

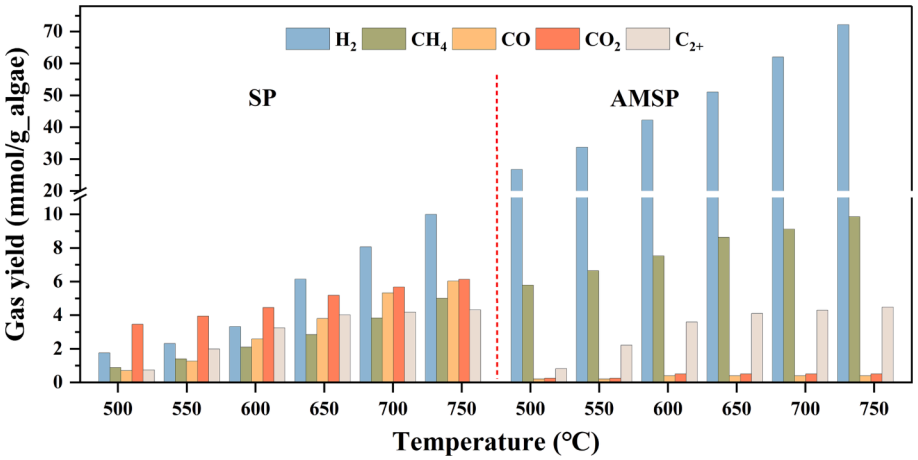


**Fig. 2.** Gas composition under different temperatures.

was applied. Finally, the obtained data was analyzed by a custom MATLAB script. More detail information about the parameter settings of instrument and the programming principles of the MATLAB script can be found in our previous work [27]. All the results were calculated based on the ash-free dry basis of algae.

## 3. Results and discussion

### 3.1. Pyrolysis products distribution

The products distribution for SP and AMSP of algae are presented in Fig. 1. In the case of SP, as the temperature increases, the gas yield increases steadily to 57.84 wt%, the char yield decreases continuously to 22.90 wt%, and the liquid yield reaches the peak of 50.06 wt% at 550 °C. The variation of liquid yield is attributed to more proteins and lipids decomposing into liquids at temperatures below 550 °C [32], while the secondary cracking of volatile at temperature above 550 °C leads to a reduction in liquid yield [14]. In the case of AMSP, the gas and liquid yield decrease to 38.77 wt% and 2.99 wt% at 750 °C, respectively, due to the reaction between $CO_X$ and molten salt reaction (2–3) and the secondary cracking of volatiles promoted by molten salt [8,20,33]. The total yield of char and soot-like is consistently below 5 wt%. With the increase of temperature, char disappears at 650 °C due to the enhanced reaction with molten NaOH-$Na_2CO_3$ reaction (3–4), while soot-like appears at 600 °C probably due to the recombination and polymerization of volatile [9,34,35]. In addition, the remaining algae substance is transferred to molten salt and its composition and transformation path were described in our previous work [8].

$$2NaOH_{(l)} + CO_{(g)} \rightarrow Na_2CO_{3(l)} + H_{2(g)} \quad (2)$$

$$4NaOH_{(l)} + C_{(s)} + CO_{2(g)} \rightarrow 2Na_2CO_{3(l)} + 2H_{2(g)} \quad (3)$$

$$C_{(s)} + Na_2CO_{3(l)} \rightarrow Na_2O_{(s)} + 2CO_{(g)} \quad (4)$$

### 3.2. Properties of gas and solid products

The composition and content of gas products at different reaction temperatures are presented in Fig. 2 and Fig. S2 respectively. Gas yield per unit weight of algae was used to compare the gas composition (especially $H_2$, CO and $CO_2$) of different processes. In the presence of molten NaOH-$Na_2CO_3$, $H_2$ yield increases sharply, $CH_4$ and $C_{2+}$ yield increase slightly, while CO and $CO_2$ production decrease sharply, which is consistent with the previous work [8]. The reduction in the pore size of the perforated plate reduces the incomplete reaction caused by the floating of small char particles during the AMSP process. As a result, $CO_X$ is almost completely consumed by molten salt (reaction (3) and (5)) [36] and its yield is less than 0.25 mmol/g-algae at the temperature studied (the $CO_X$ yield in Fig. 2 has been artificially increased to facilitate reading). As the temperature rises, the $H_2$ yield increases from 26.75 mmol/g-algae to 72.14 mmol/g-algae (750 °C), with $H_2$ accounting for 83.23 vol% of the total gas, $CH_4$ for 11.36 vol% and $C_{2+}$ for 5.17 vol%. Since $CH_4$ and $C_{2+}$ occupy a high proportion in gas products, it is desirable to convert $CH_4$ and $C_{2+}$ simultaneously by suitable means in the subsequent bio-oil reforming process to further improve hydrogen yield and purity.

$$2NaOH_{(l)} + CO_{(g)} \rightarrow Na_2CO_{3(l)} + H_{2(g)} \quad (5)$$

**Table 1**
The element composition and content of solid products produced from AMSP.

| Sample | Temperature(°C) | Elemental content (wt.%) | | | | Molar H/C |
|---|---|---|---|---|---|---|
| | | C | H | N | O* | |
| Char | 500 | 77.15 | 3.17 | 2.00 | 17.68 | 0.493 |
| | 550 | 78.40 | 2.69 | 1.87 | 17.04 | 0.412 |
| | 600 | 79.49 | 2.08 | 1.56 | 16.87 | 0.314 |
| Soot-like | 600 | 80.90 | 1.15 | 5.34 | 12.61 | 0.171 |
| | 650 | 82.73 | 0.94 | 4.46 | 11.87 | 0.136 |
| | 700 | 83.98 | 0.83 | 3.94 | 11.25 | 0.119 |
| | 750 | 84.21 | 0.77 | 3.55 | 10.54 | 0.110 |

* , by difference.

The elemental composition and content of char and soot-like produced from AMSP are listed in Table 1. Char has higher carbon content than soot-like, because char reacts with molten salt for a longer time, and $Na^+$ promotes the cleavage of C–C bond [37]. The hydrogen content of soot-like is significantly lower than that of char, implying that soot-like is formed by dehydrogenation of volatile, which is similar to the mechanism of soot formation reported in the literature [38]. Both higher temperatures and molten NaOH-$Na_2CO_3$ promote the decrease of nitrogen content of char, and the decrease of nitrogen content in soot-like may be related to the decrease of N-containing compounds in volatiles [39,40]. In addition, the molar H/C of soot-like is in the range of 0.1–0.2, slightly higher than the molar H/C (0.05–0.01) of mature soot from xylan, cellulose and lignin pyrolysis reported by Deng et al. [41]. The morphology of typical char and soot-like observed by SEM is shown in Fig. 3. It is clear that char and soot-like have quite different morphologies, char appears as irregularly stacked lamellae with broken borders due to the reaction with molten salt, while soot-like is presented as particles and spheres.

Fig. S3 shows the Raman spectrum of typical char and soot-like with the D peak (1350 $cm^{-1}$) and the G peak (1580 $cm^{-1}$) used to represent certain properties. The $I_D/I_G$, calculated from the intensity ratio of the D and G peaks, reflects the degree of graphitic disorder, and the results for char and soot-like are given in Table 2. As the temperature rises, the $I_D/I_G$ values for both char and soot-like decrease, suggesting an increase in graphitization, which matches well with the trend of molar H/C in Table 1. In addition, char has a relatively higher degree of graphitization due to its higher $I_D/I_G$ values than those of soot-like. The crystalline structure of typical char and soot-like is further revealed by the XRD as displayed in Fig. S4. Only one broadened diffraction peak (21–25°) appears on the spectrum, indicating that both char and soot-like are amorphous carbon without a three-dimensional long-range ordered structure. Compared to char, soot-like has a smaller peak angle and larger crystal spacing (according to the Bragg equation) [42], and therefore a relatively lower degree of graphitization, which is consistent with the Raman results. More information about the differences of the gas and liquid products derived from SP and AMSP as well as the related reasons can be found in our previous work [8].

### 3.3. Properties of light compounds in bio-oil

The light organic compounds in bio-oil derived from SP and AMSP are divided into eight groups, as shown in Table 3 and Table 4 respectively, and the trend of the five most abundant compounds as a function of temperature is presented in Fig. S5. For SP, the light compounds consist mainly of aliphatic hydrocarbons (3.20–29.20 area %), N-heterocyclic aromatic compounds (21.96–27.86 area %) and aromatic hydrocarbons (6.08–65.27 area %), with the most abundant compounds being p-cresol, naphthalene, anthracene, pyrene and indole. For AMSP,

**Table 2**
The $I_D/I_G$ values based on the Raman spectra of char and soot-like.

| Sample | Temperature(°C) | $I_D/I_G$ | | |
|---|---|---|---|---|
| | | Value | Error (−) | Error (+) |
| Char | 500 | 0.884 | 0.018 | 0.013 |
| | 550 | 0.851 | 0.024 | 0.015 |
| | 600 | 0.834 | 0.022 | 0.017 |
| Soot-like | 600 | 0.916 | 0.017 | 0.025 |
| | 650 | 0.905 | 0.018 | 0.020 |
| | 700 | 0.895 | 0.014 | 0.015 |
| | 750 | 0.884 | 0.019 | 0.009 |

**Table 3**
The main groups of light organic compounds for SP.

| Classification | Content (area %) | | | | | |
|---|---|---|---|---|---|---|
| | 500 °C | 550 °C | 600 °C | 650 °C | 700 °C | 750 °C |
| Aliphatic hydrocarbons | 29.20 | 22.83 | 20.78 | 12.57 | 7.34 | 3.20 |
| Linear alkanes | 10.68 | 7.52 | 5.61 | 2.37 | 1.07 | 0.60 |
| Linear alkenes | 18.53 | 15.31 | 15.16 | 10.20 | 6.27 | 2.40 |
| Aromatic hydrocarbons | 6.08 | 9.70 | 19.50 | 45.20 | 56.64 | 65.27 |
| Alicyclic hydrocarbons | 11.95 | 13.60 | 11.06 | 2.42 | – | – |
| N-heterocyclic aromatic compounds | 25.43 | 27.86 | 21.96 | 23.18 | 24.12 | 23.68 |
| Amines/amides | 5.17 | 4.21 | 4.45 | 1.42 | – | – |
| Nitriles | 8.99 | 9.31 | 8.29 | 5.69 | 5.50 | 3.55 |
| Phenols | 1.39 | 5.50 | 10.61 | 7.32 | 4.69 | 3.11 |
| Oxygenated compounds* | 11.80 | 6.99 | 3.36 | 2.21 | 1.71 | 1.19 |

* consisting of alcohols, carboxylic acids, esters and aldehydes; -, not detected.

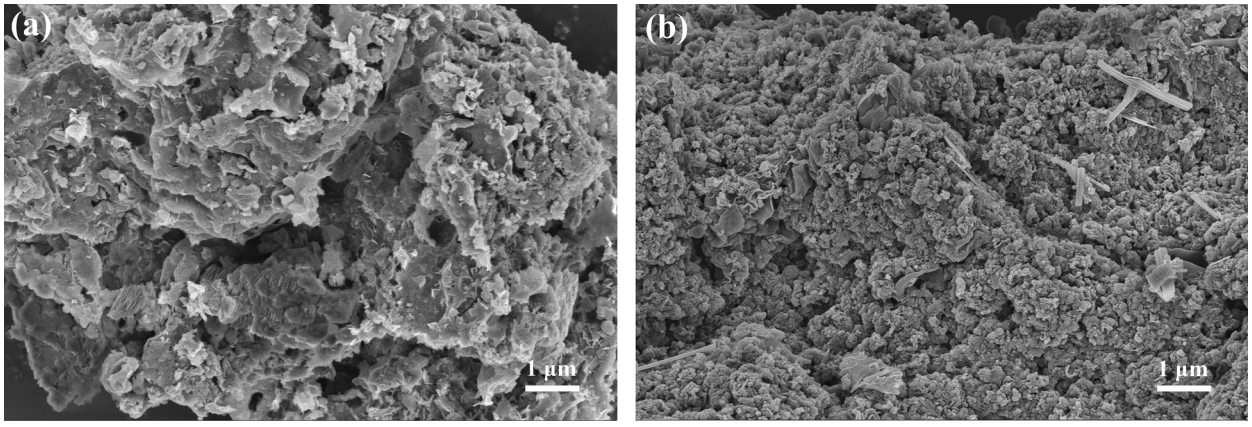


**Fig. 3.** FE-SEM images of (a) char obtained at 500 °C and (b) soot-like obtained at 750 °C.

**Table 4**
The main groups of light organic compounds for AMSP.

| Classification | Content (area %) | | | | | |
|---|---|---|---|---|---|---|
| | 500 °C | 550 °C | 600 °C | 650 °C | 700 °C | 750 °C |
| Aliphatic hydrocarbons | 36.60 | 27.56 | 10.69 | 2.57 | 2.13 | 1.11 |
| Linear alkanes | 12.39 | 8.13 | 6.51 | 2.57 | 2.13 | 1.11 |
| Linear alkenes | 24.21 | 19.43 | 4.18 | – | – | – |
| Aromatic hydrocarbons | 19.99 | 26.15 | 55.44 | 59.36 | 63.40 | 64.06 |
| Alicyclic hydrocarbons | 12.47 | 9.26 | 2.78 | – | – | – |
| N-heterocyclic aromatic compounds | 8.71 | 7.93 | 2.80 | – | – | – |
| Amines/amides | 5.49 | 4.32 | – | – | – | – |
| Nitriles | 9.91 | 9.11 | 1.64 | – | – | – |
| Phenols | 2.07 | 8.32 | 18.30 | 20.65 | 29.33 | 31.44 |
| Oxygenated compounds* | 4.76 | 7.35 | 8.35 | 17.43 | 5.17 | 3.40 |

* consisting of alcohols, carboxylic acids, esters and aldehydes; -, not detected.

aliphatic hydrocarbons (1.11–36.60 area %), phenols (2.07–31.44 area %) and aromatic hydrocarbons (19.99–64.06 area %) are the major components of light compounds, and the most abundant compounds are 2,2′-methylenebi(4-methyl-6-*tert*-butylphenol), 2-methylnaphthalen, naphthalene, cholesta-3,5-diene and dimethyl phthalate.

The aliphatic hydrocarbons are divided into linear alkanes (e.g., pentadecane) and linear alkenes (e.g., 1-octadecene). With the increase of temperature, the linear alkanes and linear alkanes decrease continuously in content, possibly because higher temperatures promote their cracking to non-condensable gases (e.g., $C_2H_2$) or their aromatization to form aromatics [43,44]. Molten NaOH-$Na_2CO_3$ contributes little to alkanes conversion, but promotes alkenes conversion dramatically at temperatures higher than 550 °C, due to the fact that alkenes are more reactive than alkanes. Since only the content of aromatic hydrocarbons and oxygenated compounds increases above 550 °C, it is presumed that molten salt intensifies the aromatization or oxidation of linear alkenes.

The content of N-heterocyclic aromatic compounds (e.g., indole) for AMSP is significantly reduced (dropping to zero above 600 °C) compared to that for SP. Studies have shown that the N-heterocyclic aromatic compounds in bio-oil are mainly derived from the cracking of amino acids, as well as the secondary cracking of pyridine-N and pyrrole-N in char [45,46]. Reactions between molten NaOH-$Na_2CO_3$ and amino acids may be the main reason for the decrease in the content of N-heterocyclic aromatic compounds [47]. In addition, the above reactions are also responsible for the conversion of nitriles and amines/amides at temperatures above 600 °C, as nitriles and amines/amides are mainly derived from the conversion of protein fragments (amino acids and peptides) and the dehydration of amides [46,48].

The higher content of aromatic hydrocarbons for AMSP implies that molten NaOH-$Na_2CO_3$ promotes the hydrogen formation from the aromatization of light compounds. According to the number of benzene rings, the aromatics hydrocarbons are further categorized as one/two/three/four/five-rings aromatics to show the relationship between the composition of aromatics hydrocarbons and the hydrogen yield at different temperatures (Fig. 4). In the presence or absence of molten salt, the main compounds are essentially the same, such as naphthalene, 2-methylnaphthalene, anthracene and pyrene. At 550 °C, the one-ring aromatics (e.g., toluene) can be formed from the long-chain fatty acids by C–C bond breaking, cyclization and aromatization [14], and the two-ring aromatics (mainly naphthalene) may be evolved from benzene through the fusion of alicyclic hydrocarbons [49]. As temperature rises, the aromatization of aromatics with fewer rings intensifies to form aromatics with more rings and release large amounts of hydrogen [20]. Compared with SP, the content of aromatics with fewer rings (one and/or two rings) from AMSP decreases, while that of aromatics with more rings (three, four and five rings) increases at temperatures above 600 °C. The aromatics with more rings in the volatile tend to condense (forming condensed aromatics in heavy compounds, refer to 3.4) and grow to form soot-like eventually at higher temperatures. On the other hand, $Na^+$ in molten salt can promote the conversion of small aromatic ring systems to large aromatic ring systems, while the high heating rate provided by molten salt has the opposite effect [26,50].

For the phenolic compounds, molten salt significantly increases the relative content of phenol especially at higher temperatures, and the content of phenols reaches 31.44 area % at 750 °C, including 30.45 area % for 2,2′-methylenebis(4-methyl-6-*tert*-butylphenol) and 0.99 area %

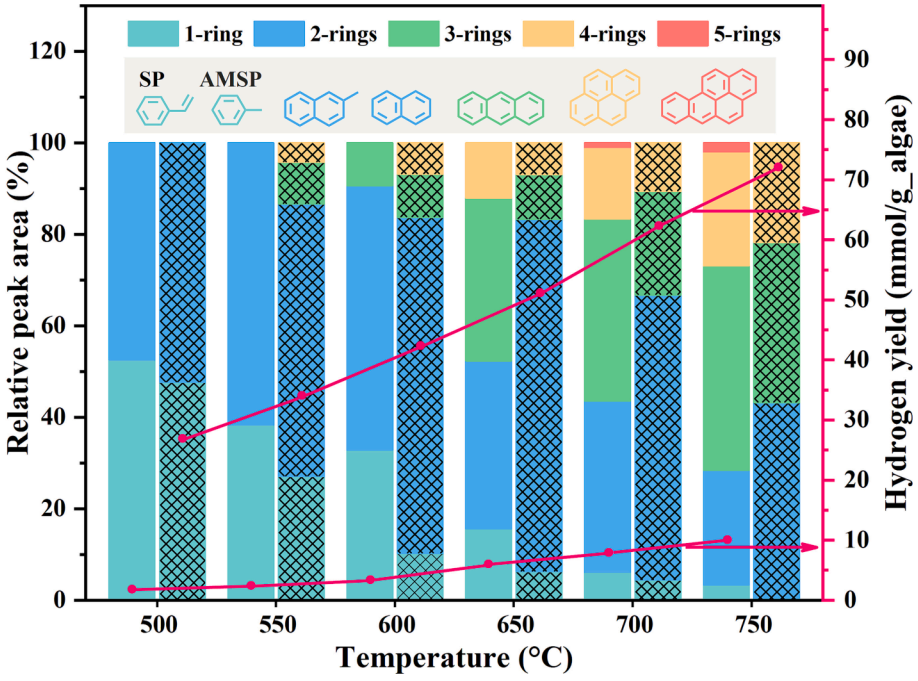


**Fig. 4.** The relationship between the composition of aromatics hydrocarbons and hydrogen yield (entity: SP, shadow: AMSP).

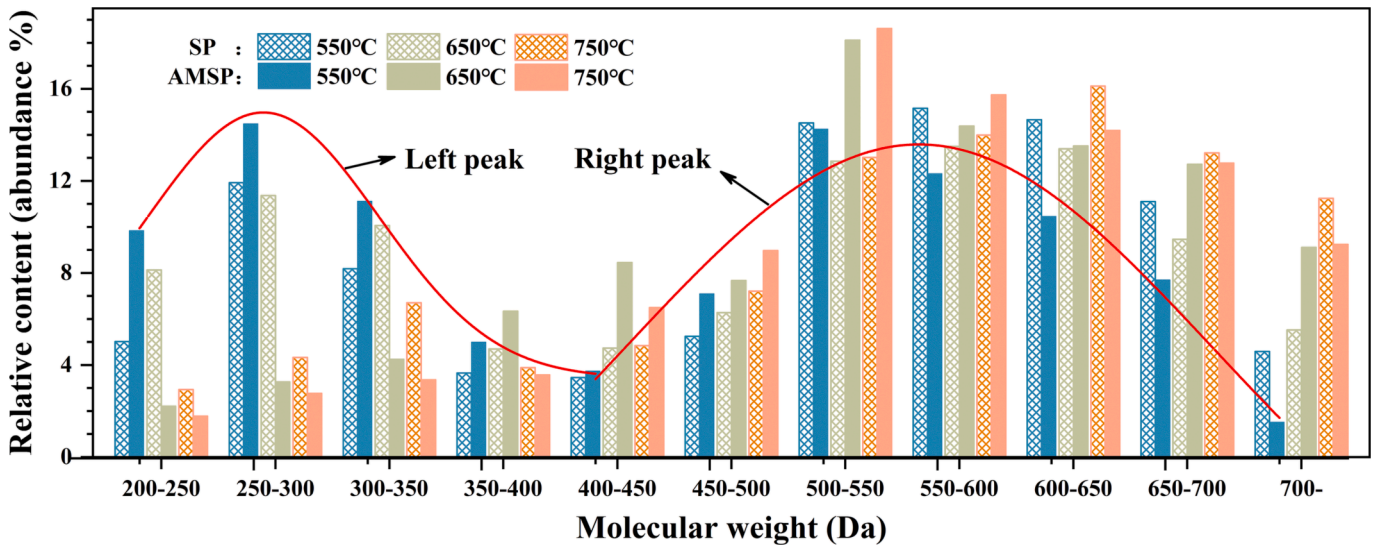


**Fig. 5.** The molecular weight distribution of heavy components.

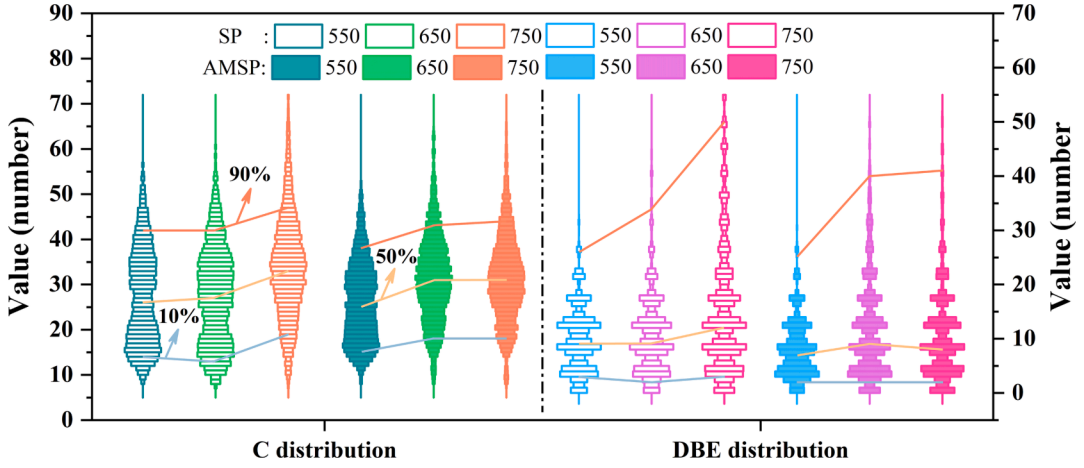


**Fig. 6.** The distributions of CN and DBE in heavy components (50% line represents the median line, and the rest parameters are similar in principle).

for 3,5-bis(*tert*-butylphenol). The existing studies have shown that the decarbonation by carbonate promotes the formation of methoxyphenols, and $OH^-$ can further promote the deoxygenation of methoxyphenols to form alkylphenols or phenols [51,52]. Moreover, it has found that methoxyphenols can be completely converted to alkylphenols in molten salt (monomer of 2,2′-methylenebis(4-methyl-6-*tert*-butylphenol)) at temperatures above 450 °C in our previous study [20]. Therefore, large quantities of 2,2′-methylenebi(4-methyl-6-*tert*-butylphenol) with high purity was produced by the polymerization of alkylphenols (3,5-bis(*tert*-butylphenol)) with the effect of molten NaOH-$Na_2CO_3$, while releasing a certain amount of $CH_4$ [53,54].

### 3.4. Properties of heavy compounds in bio-oil

Fig. 5 presents the molecular weight distribution of heavy components in bio-oil at different temperatures. Overall, the heavy components show a bimodal distribution (as shown as the red lines representing AMSP550) in molecular weight, and the components with molecular weight greater than 500 Da are more abundant, especially at higher temperatures. As the temperature increases, the molecular weights of the left and right peaks of SP increase slowly from 250 to 300 Da and 550–600 Da to 300–350 Da and 600–650 Da, respectively. And for AMSP, the molecular weight of the left peak increases sharply from 250 to 300 Da to approximately 500–550 Da, and that of the right peak remains roughly unchanged (500–550 Da). Molten salt enhances the polymerization (which is also promoted by higher temperatures) of heavy components with smaller molecular weight, while promote the decomposition of heavy components with larger molecular weight, which is attributed by the integrated effect of $Na^+$, high heating rate and soot-like formation [26,35,50].

The distributions of carbon atoms and double bond equivalents (DBE) of heavy components are presented in Fig. 6 to evaluate the core structure of detected species. DBE is an essential index used to evaluate the unsaturation of compounds, and its calculation method was reported elsewhere [55]. It can be noticed that most of the heavy compounds (from the 10 % line and 90 % line) have carbon atoms number (CN) and DBE mainly distributed between 13 and 47 and 2–50, respectively, for both SP and AMSP. There is an overall upward trend (as illustrated by the 50 % line) in both CN and DBE as the temperature rises, suggesting a stronger condensation associated with unsaturated carbon bonds occurs at higher temperatures. The addition of molten salt reduces the growth rate of CN and DBE at temperature higher than 650 °C, suggesting that molten NaOH-$Na_2CO_3$ can inhibit the condensation of heavy components at higher temperatures (this result can also be illustrated by the Van Krevelen diagrams below).

CHO compounds and nitrogen-containing compounds (both present

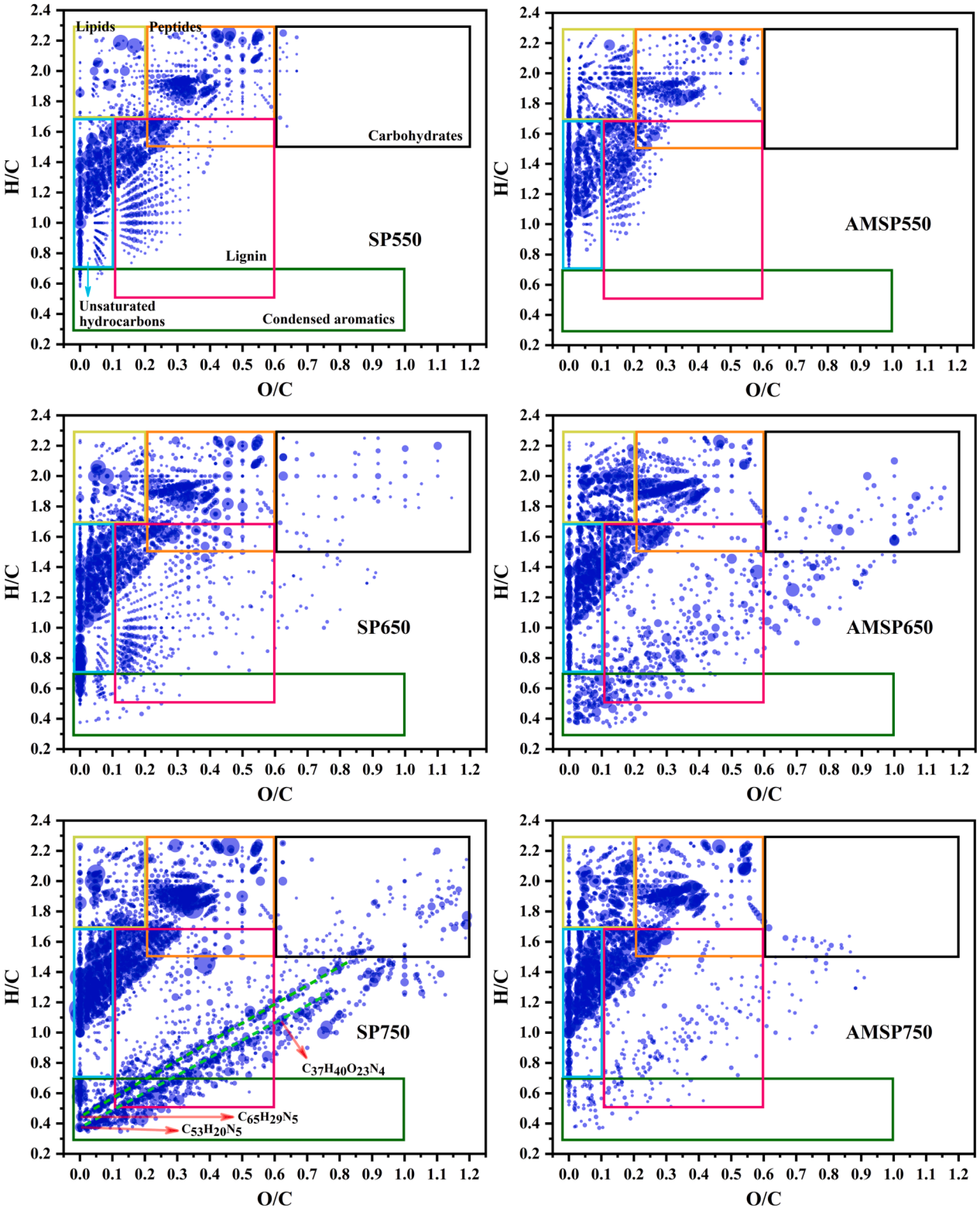


**Fig. 7.** Van Krevelen diagrams of heavy components in bio-oil.

at high levels in bio-oil) could affect the catalyst activity in the bio-oil reforming process [56,57], so the content of CHO compounds as well as the average nitrogen number (ANN) in heavy components are calculated (the method can be found in [27]) with the results listed in Table S2. Obviously, SP and AMSP share a similar trend in CHO content and ANN. With the increase of temperature, the ANN increases, while the CHO content remains basically unchanged. Overall, molten NaOH-$Na_2CO_3$ contributes slightly to the removal of nitrogen, as well as the formation of CHO compounds, suggesting that the available catalysts for bio-oil (derived from SP) reforming can be referenced for AMSP process when only the heavy compounds are considered.

The heavy components are further plotted in the Van Krevelen diagram based on their elemental composition (O/C and H/C value), with the size of circles representing the abundance of each compound, as

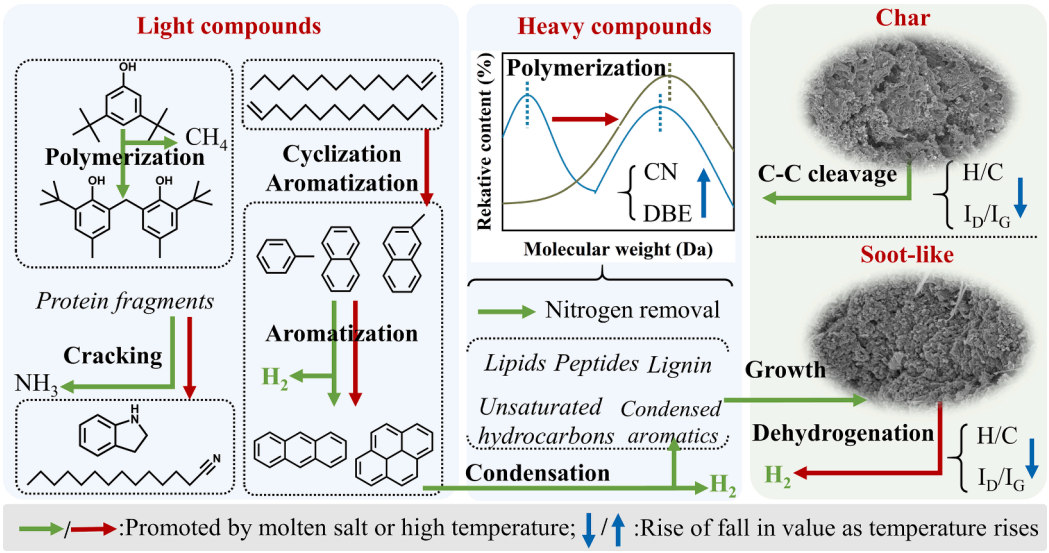


**Fig. 8.** Transformation pathways of pyrolysis products in molten NaOH-$Na_2CO_3$.

shown in Fig. 7. With reference to the existing literatures [27,58], the heavy components are mainly divided into lipids, unsaturated hydrocarbons, peptides, lignin, condensed aromatics and carbohydrates.

For SP, the major compounds are composed of lipids, unsaturated hydrocarbons and lignin at 550 °C and 650 °C, and more condensed aromatics are formed at 750 °C due to the aromatization (e.g., hydrocarbons aromatization, refer to the line of O/C = 0), which is promoted by high temperature. Besides, a large number of new compounds are produced at 750 °C, which is linearly distributed on the Van Krevelen diagram, as shown as the green lines. It is speculated that these compounds are formed by a combination of the deoxygenation of carbohydrates (due to the presence of a diffusion points with O/C = 1, H/C ≈ 1.6) and the oxidation of nitrogen-containing polycyclic compounds (e.g., $C_{65}H_{29}N_5$ and $C_{50}H_{20}N_5$) at higher temperatures.

For AMSP, the addition of molten salt seems to facilitate the pyrolysis process, as AMSP650 and SP750 share a very similar Van Krevelen diagram, especially the region where the green lines are located and the disappearance of stretching lines associated with the diffusion point (O/C = 0, H/C = 1). This is because molten salt accelerates the heat transfer from the surface to interior of the algae pellet, greatly reducing the temperature gradient inside the pellet. It is clear that there are more heavy compounds belonging to the region of lipids, which was reported to mainly consist of fatty acids, resin acids and other wood extractives [59]. The main conversion pathways for heavy fatty acids are chain-breaking and cyclization [14], but the acid content detected by GC–MS for both SP and AMSP is low, suggesting that molten NaOH-$Na_2CO_3$ inhibits the cyclization rather than chain-breaking of large fatty acids.

### 3.5. Transformation pathways of pyrolysis products

The transformation pathways of pyrolysis products related to hydrogen-containing gases release in molten NaOH-$Na_2CO_3$ are proposed based on the above discussions (shown in Fig. 8). The light compounds in bio-oil consist mainly of aliphatic hydrocarbons, phenols and aromatic hydrocarbons, and the content of phenols and aromatic hydrocarbons reaches up to 95.5 % at 750 °C. Linear alkenes of aliphatic hydrocarbons tend to form aromatics with $H_2$ release through cyclization and aromatization above 550 °C. Alkylphenols (3,5-bis(*tert*-butylphenol) are produced by the decarbonation of $Na_2CO_3$ and the deoxygenation of NaOH, and are subsequently converted into 2,2′-methylenebi(4-methyl-6-*tert*-butylphenol) by polymerization with $CH_4$ release. Besides, molten salt promotes the cracking of protein fragments (e.g. amino acids) into $NH_3$, substantially reducing the nitrogen-containing compounds derived from these protein fragments.

The heavy compounds consist mainly of lipids, peptides, lignin and unsaturated hydrocarbons. As temperature rises, the heavy compounds undergo polymerization to form compounds with higher molecular weights and higher unsaturation, leading to an increase in CN and DBE. Char reacts with molten salt to form $H_2$ and disappears at 650 °C, while aromatics in light compounds condense into heavy compounds, which then grow to form soot-like and release $H_2$ at 600 °C. Moreover, molten salt promotes the cleavage of C–C bonds in char, leading to a lower carbon content in char than that in soot-like, while higher temperatures enhance the dehydrogenation of soot-like, resulting in a decrease in molar H/C and $I_D/I_G$ values.

### 3.6. Future development of AMSP

In order to further improve the hydrogen yield and purity production by the AMSP of algae, impurity gases and bio-oil vapors entrained in the hydrogen-rich gas need to be removed or converted as much as possible. In terms of gas composition, despite the high hydrogen yield and purity (72.14 mmol/g-algae and 83.23 vol%) obtained, 11.36 vol% $CH_4$ and 5.17 vol% $C_{2+}$ are still contained in the gas product. Therefore, it is desirable to convert $CH_4$ and $C_{2+}$ simultaneously during the AMSP process to further improve hydrogen yield and purity, such as steam reforming. In terms of bio-oil composition, the higher aromatic and phenolic content (95.5 %) allows Ni-based catalysts (e.g., Ni-$ZrO_2$, Ni-MgO, etc.) suitable for bio-oil steam reforming, because these Ni-based catalysts have significant capacity for C–C,C–H and O–H bond cleavage [60,61]. In addition, the content of active CHO compounds and nitrogenous compounds in the heavy bio-oil obtained from ASMP changes little compared to that obtained from SP, suggesting that conventional catalysts considering carbon deposition or poisoning are applicable for the bio-oil cleaning process of AMSP.

## 4. Conclusion

Algae pyrolysis in molten NaOH-$Na_2CO_3$ produces 72.14 mmol/g-algae of $H_2$ at 750 °C with a purity of 83.23 vol%. As the temperature rises from 500 °C to 750 °C, char reacts with molten salt and disappears at 650 °C, while aromatics in light compounds condense into heavy compounds and then grow to form soot-like at 600 °C, both processes releasing large amounts of $H_2$. Molten salt promotes the cyclization/aromatization of linear alkenes and the cracking of protein fragments

into $NH_3$. Alkylphenols are produced via the decarbonation by $Na_2CO_3$ and deoxygenation by NaOH, and then further polymerized to release $CH_4$. The heavy bio-oil compounds, with CN and DBE mainly in regions of 18–44 and 2–41. As the temperature increases, these components tend to polymerize into compounds with higher molecular weights and unsaturation, leading to an increase in CN and DBE. Based on the products transformation, the ex-situ steam reforming processes using Ni-based catalysts are proposed to further improve the hydrogen yield and purity.

## CRediT authorship contribution statement

**Jun Li:** Writing – original draft, Visualization, Methodology, Conceptualization. **Kuo Zeng:** Writing – review & editing, Project administration, Formal analysis. **Dian Zhong:** Methodology, Formal analysis, Conceptualization. **Xin Chen:** Software, Methodology. **Ange Nzihou:** Writing – review & editing, Supervision. **Haiping Yang:** Supervision, Resources, Formal analysis. **Hanping Chen:** Supervision, Resources, Formal analysis.

## Declaration of Competing Interest

The authors declare that they have no known competing financial interests or personal relationships that could have appeared to influence the work reported in this paper.

## Data availability

Data will be made available on request.

## Acknowledgement

Authors acknowledge funding from the National Natural Science Foundation of China (52261135626, 52111530296, 52076098), and the support of National Natural Science Funds for Distinguished Young Scholar (52125601). In addition, authors would like to thank the Analytical and Testing Center in Huazhong University of Science & Technology (http://atc.hust.edu.cn) and the shiyanjia lab (https://www.shiyanjia.com) for the test. There are no conflicts to declare.

## Appendix A. Supplementary data

Supplementary data to this article can be found online at https://doi.org/10.1016/j.fuel.2023.129868.

## References

[1] Xu Z, Ma X, Zhou J, Duan P, Zhou W, Ahmad A, et al. The influence of key reactions during hydrothermal carbonization of sewage sludge on aqueous phase properties: a review. Journal of Analytical and Applied Pyrolysis 2022;167:105678. https://doi.org/10.1016/j.jaap.2022.105678.
[2] Xu Z, Song H, Li P, He Z, Wang Q, Wang K, et al. Hydrothermal carbonization of sewage sludge: effect of aqueous phase recycling. Chemical Engineering Journal 2020;387:123410. https://doi.org/10.1016/j.cej.2019.123410.
[3] Choi J, Choi J, Suh DJ, Ha J, Hwang JW, Jung HW, et al. Production of brown algae pyrolysis oils for liquid biofuels depending on the chemical pretreatment methods. Energy Convers Manag 2014;86:371–8. https://doi.org/10.1016/j.enconman.2014.04.094.
[4] Kouhgardi E, Zendehboudi S, Mohammadzadeh O, Lohi A, Chatzis I. Current status and future prospects of biofuel production from brown algae in north america: progress and challenges. Renewable and Sustainable Energy Reviews 2023;172:113012. https://doi.org/10.1016/j.rser.2022.113012.
[5] Wang X, Zhang Y, Xia C, Alqahtani A, Sharma A, Pugazhendhi A. A review on optimistic biorefinery products: biofuel and bioproducts from algae biomass. Fuel 2023;338:127378. https://doi.org/10.1016/j.fuel.2022.127378.
[6] Zeng K, Li R, Minh DP, Weiss-Hortala E, Nzihou A, He X, et al. Solar pyrolysis of heavy metal contaminated biomass for gas fuel production. Energy 2019;187:116016. https://doi.org/10.1016/j.energy.2019.116016.
[7] Yang J, Zhao T, Cui X, Peng M, Wang X, Mao H, et al. New insights into the carbon neutrality of microalgae from culture to utilization: a critical review on the algae-based solid biofuels. Biomass and Bioenergy 2022;166:106599. https://doi.org/10.1016/j.biombioe.2022.106599.
[8] Li J, Zeng K, Zhong D, Flamant G, Nzihou A, White CE, et al. Algae pyrolysis in molten NaOH-$Na_2CO_3$ for hydrogen production. Environmental Science & Technology 2023;57(16):6485–93. https://doi.org/10.1021/acs.est.3c01325.
[9] Cherad R, Onwudili JA, Biller P, Williams PT, Ross AB. Hydrogen production from the catalytic supercritical water gasification of process water generated from hydrothermal liquefaction of microalgae. Fuel 2016;166:24–8. https://doi.org/10.1016/j.fuel.2015.10.088.
[10] Duman G, Uddin MA, Yanik J. Hydrogen production from algal biomass via steam gasification. Bioresource Technology 2014;166:24–30. https://doi.org/10.1016/j.biortech.2014.04.096.
[11] Lin KC, Lin Y, Hsiao Y. Microwave plasma studies of spirulina algae pyrolysis with relevance to hydrogen production. Energy 2014;64:567–74. https://doi.org/10.1016/j.energy.2013.09.055.
[12] Xie Y, Yang H, Zeng K, Zhu Y, Hu J, Mao Q, et al. Study on $CO_2$ gasification of biochar in molten salts: reactivity and structure evolution. Fuel 2019;254:115614. https://doi.org/10.1016/j.fuel.2019.06.022.
[13] Li J, Xie Y, Zeng K, Flamant G, Yang H, Yang X, et al. Biomass gasification in molten salt for syngas production. Energy 2020;210:118563. https://doi.org/10.1016/j.energy.2020.118563.
[14] Chen W, Yang H, Chen Y, Xia M, Yang Z, Wang X, et al. Algae pyrolytic poly-generation: influence of component difference and temperature on products characteristics. Energy 2017;131:1–12. https://doi.org/10.1016/j.energy.2017.05.019.
[15] Ishida M, Otsuka K, Takenaka S, Yamanaka I. One-step production of co- and co2-free hydrogen from biomass. Journal of Chemical Technology and Biotechnology 2005;80(3):281–4. https://doi.org/10.1002/jctb.1188.
[16] Yin H, Lu B, Xu Y, Tang D, Mao X, Xiao W, et al. Harvesting capacitive carbon by carbonization of waste biomass in molten salts. Environmental Science & Technology 2014;48(14):8101–8. https://doi.org/10.1021/es501739v.
[17] Xiong Z, Syed-Hassan SSA, Hu X, Guo J, Chen Y, Liu Q, et al. Effects of the component interaction on the formation of aromatic structures during the pyrolysis of bio-oil at various temperatures and heating rates. Fuel 2018;233:461–8. https://doi.org/10.1016/j.fuel.2018.06.064.
[18] Xiong Z, Syed-Hassan SSA, Xu J, Wang Y, Hu S, Su S, et al. Evolution of coke structures during the pyrolysis of bio-oil at various temperatures and heating rates. Journal of Analytical and Applied Pyrolysis 2018;134:336–42. https://doi.org/10.1016/j.jaap.2018.06.023.
[19] Xu K, Li J, Zeng K, Zhong D, Peng J, Qiu Y, et al. The characteristics and evolution of nitrogen in bio-oil from microalgae pyrolysis in molten salt. Fuel 2023;331:125903. https://doi.org/10.1016/j.fuel.2022.125903.
[20] Zeng K, Li J, Xie Y, Yang H, Yang X, Zhong D, et al. Molten salt pyrolysis of biomass: the mechanism of volatile reforming and pyrolysis. Energy 2020;213:118801. https://doi.org/10.1016/j.energy.2020.118801.
[21] Ratchahat S, Kodama S, Tanthapanichakoon W, Sekiguchi H. Combined molten salt–Ni/$Al_2O_3$ as synergistic medium for high-quality syngas production. Chemical Engineering Journal 2015;278:224–33. https://doi.org/10.1016/j.cej.2014.09.109.
[22] Kumar R, Strezov V, Weldekidan H, He J, Singh S, Kan T, et al. Lignocellulose biomass pyrolysis for bio-oil production: a review of biomass pre-treatment methods for production of drop-in fuels. Renewable and Sustainable Energy Reviews 2020;123:109763. https://doi.org/10.1016/j.rser.2020.109763.
[23] Shashkov MV, Sotnikova YS, Dolgushev PA, Alekseeva MV. Development of comprehensive analysis of pyrolysis products for lignocellulose raw materials and sludge sediments by chromatographic methods. Journal of Siberian Federal University Chemistry 2021;14(4):489–501. https://doi.org/10.17516/1998-2836-0240.
[24] Ye X, Zou X, Tian F, He H. Feasibility study on recycled vegetable oil waste and recycled polyethylene for the modification of aged asphalt. PLoS One1 2021;16(1):e244159. https://doi.org/10.1371/journal.pone.0244159.
[25] Chaiwong K, Kiatsiriroat T, Vorayos N, Thararax C. Study of bio-oil and bio-char production from algae by slow pyrolysis. Biomass and Bioenergy 2013;56:600–6. https://doi.org/10.1016/j.biombioe.2013.05.035.
[26] Xiong Z, Guo J, Han H, Xu J, Jiang L, Su S, et al. Effects of aaems on formation of heavy components in bio-oil during pyrolysis at various temperatures and heating rates. Fuel Processing Technology 2021;213:106690. https://doi.org/10.1016/j.fuproc.2020.106690.
[27] Li J, Xiong Z, Zeng K, Zhong D, Zhang X, Chen W, et al. Characteristics and evolution of nitrogen in the heavy components of algae pyrolysis bio-oil. Environmental Science & Technology 2021;55(9):6373–85. https://doi.org/10.1021/acs.est.1c00676.
[28] Zhong D, Zeng K, Li J, Qiu Y, Flamant G, Nzihou A, et al. Characteristics and evolution of heavy components in bio-oil from the pyrolysis of cellulose, hemicellulose and lignin. Renewable and Sustainable Energy Reviews 2022;157:111989. https://doi.org/10.1016/j.rser.2021.111989.
[29] Qiu Y, Zhong D, Zeng K, Li J, Flamant G, Nzihou A, et al. Effects of cellulose-lignin interaction on the evolution of biomass pyrolysis bio-oil heavy components. Fuel 2022;323:124413. https://doi.org/10.1016/j.fuel.2022.124413.
[30] Pooja M, Ravishankar KS, Madav V. High temperature corrosion behaviour of stainless steels and inconel 625 in hydroxide salt. Materials Today: Proceedings 2021;46:2612–5. https://doi.org/10.1016/j.matpr.2021.02.266.
[31] Yin H, Zhou Y, Liu Q, Wang Y, Tang Z, Yan L. Corrosion behavior and mechanism of gh3535 alloy in naoh, hf and h2o2 solution. Journal of Alloys and Compounds 2021;887:161387. https://doi.org/10.1016/j.jallcom.2021.161387.
[32] Wang X, Sheng L, Yang X. Pyrolysis characteristics and pathways of protein, lipid and carbohydrate isolated from microalgae nannochloropsis sp. Bioresource Technology 2017;229:119–25. https://doi.org/10.1016/j.biortech.2017.01.018.

[33] Ishida M, Takenaka S, Yamanaka I, Otsuka K. Production of cox-free hydrogen from biomass and naoh mixture: effect of catalysts. Energy & Fuels: An American Chemical Society Journal 2006;20(2):748–53. https://doi.org/10.1021/ef050282u.
[34] Nagase K, Shimodaira T, Itoh M, Zheng Y. Kinetics and mechanisms of the reverse boudouard reaction over metal carbonates in connection with the reactions of solid carbon with the metal carbonates. Physical Chemistry Chemical Physics 1999;1(24):5659–64. https://doi.org/10.1039/A906687J.
[35] Trubetskaya A, Jensen PA, Jensen AD, Garcia Llamas AD, Umeki K, Gardini D, et al. Effects of several types of biomass fuels on the yield, nanostructure and reactivity of soot from fast pyrolysis at high temperatures. Applied Energy 2016;171:468–82. https://doi.org/10.1016/j.apenergy.2016.02.127.
[36] Ferguson TE, Park Y, Petit C, Park AA. Novel approach to hydrogen production with suppressed cox generation from a model biomass feedstock. Energy & Fuels: An American Chemical Society Journal 2012;26(7):4486–96. https://doi.org/10.1021/ef300653b.
[37] Di Blasi C, Galgano A, Branca C. Influences of the chemical state of alkaline compounds and the nature of alkali metal on wood pyrolysis. Industrial and Engineering Chemistry Research 2009;48(7):3359–69. https://doi.org/10.1021/ie801468y.
[38] Wang X, Li Y, Bai S, Jin Q, Mikulčić H, Tan H, et al. Nano-scale soot particle formation during the high-temperature pyrolysis of waste plastics in an entrained flow reactor. Waste and Biomass Valorization 2019;10(12):3857–66. https://doi.org/10.1007/s12649-018-0322-x.
[39] Tay T, Ucar S, Karagöz S. Preparation and characterization of activated carbon from waste biomass. Journal of Hazardous Materials 2009;165(1):481–5. https://doi.org/10.1016/j.jhazmat.2008.10.011.
[40] Li J, Peng J, Zeng K, Zhong D, Xu K, Vladimirovich VS, et al. Solar pyrolysis of algae in molten salt for capacitive carbon preparation. Journal of Cleaner Production 2023;406:136898. https://doi.org/10.1016/j.jclepro.2023.136898.
[41] Deng C, Liaw SB, Gao X, Wu H. Differences in soot produced from rapid pyrolysis of xylan, cellulose and lignin under pulverized-fuel conditions. Fuel 2020;265:116991. https://doi.org/10.1016/j.fuel.2019.116991.
[42] Lu L, Kong C, Sahajwalla V, Harris D. Char structural ordering during pyrolysis and combustion and its influence on char reactivity. Fuel 2002;81(9):1215–25. https://doi.org/10.1016/S0016-2361(02)00035-2.
[43] Baldwin RM, Magrini-Bair KA, Nimlos MR, Pepiot P, Donohoe BS, Hensley JE, et al. Current research on thermochemical conversion of biomass at the national renewable energy laboratory. Applied Catalysis. B, Environmental 2012;115–116:320–9. https://doi.org/10.1016/j.apcatb.2011.10.033.
[44] Ledesma EB, Kalish MA, Nelson PF, Wornat MJ, Mackie JC. Formation and fate of pah during the pyrolysis and fuel-rich combustion of coal primary tar. Fuel 2000;79(14):1801–14. https://doi.org/10.1016/S0016-2361(00)00044-2.
[45] Chen Y, Wu Y, Hua D, Li C, Harold MP, Wang J, et al. Thermochemical conversion of low-lipid microalgae for the production of liquid fuels: challenges and opportunities. RSC Advances 2015;5(24):18673–701. https://doi.org/10.1039/C4RA13359E.
[46] Debono O, Villot A. Nitrogen products and reaction pathway of nitrogen compounds during the pyrolysis of various organic wastes. Journal of Analytical and Applied Pyrolysis 2015;114:222–34. https://doi.org/10.1016/j.jaap.2015.06.002.
[47] Chen H, Shan R, Zhao F, Gu J, Zhang Y, Yuan H, et al. A review on the nox precursors release during biomass pyrolysis. Chemical Engineering Journal 2023;451:138979. https://doi.org/10.1016/j.cej.2022.138979.
[48] Chen W, Yang H, Chen Y, Xia M, Chen X, Chen H. Transformation of nitrogen and evolution of n-containing species during algae pyrolysis. Environmental Science & Technology 2017;51(11):6570–9. https://doi.org/10.1021/acs.est.7b00434.
[49] Bensabath T, Le MD, Monnier H, Glaude P. Polycyclic aromatic hydrocarbon (PAH) formation during acetylene pyrolysis in tubular reactor under low pressure carburizing conditions. Chemical Engineering Science 2019;202:84–94. https://doi.org/10.1016/j.ces.2019.03.030.
[50] Xiong Z, Guo J, Chaiwat W, Deng W, Hu X, Han H, et al. Assessing the chemical composition of heavy components in bio-oils from the pyrolysis of cellulose, hemicellulose and lignin at slow and fast heating rates. Fuel Processing Technology 2020;199:106299. https://doi.org/10.1016/j.fuproc.2019.106299.
[51] özbay G, Koçak E, Ahmad MS. Pyrolysis of water buffalo manure: influence of temperature and alkali hydroxide additives on the quality of bio-oil. Biocatalysis and Agricultural Biotechnology 2021;38.
[52] Peng C, Zhang G, Yue J, Xu G. Pyrolysis of lignin for phenols with alkaline additive. Fuel Processing Technology 2014;124:212–21. https://doi.org/10.1016/j.fuproc.2014.02.025.
[53] Xie Y, Zeng K, Flamant G, Yang H, Liu N, He X, et al. Solar pyrolysis of cotton stalk in molten salt for bio-fuel production. Energy 2019;179:1124–32. https://doi.org/10.1016/j.energy.2019.05.055.
[54] Stefanidis SD, Kalogiannis KG, Iliopoulou EF, Lappas AA, Pilavachi PA. In-situ upgrading of biomass pyrolysis vapors: catalyst screening on a fixed bed reactor. Bioresource Technology 2011;102(17):8261–7. https://doi.org/10.1016/j.biortech.2011.06.032.
[55] Koch BP, Witt M, Engbrodt R, Dittmar T, Kattner G. Molecular formulae of marine and terrigenous dissolved organic matter detected by electrospray ionization fourier transform ion cyclotron resonance mass spectrometry. Geochimica et Cosmochimica Acta 2005;69(13):3299–308. https://doi.org/10.1016/j.gca.2005.02.027.
[56] Xiong Z, Xiong Y, Li Q, Han H, Deng W, Xu J, et al. Effects of vapor-/solid-phase interactions among cellulose, hemicellulose and lignin on the formation of heavy components in bio-oil during pyrolysis. Fuel Processing Technology 2022;225:107042. https://doi.org/10.1016/j.fuproc.2021.107042.
[57] Binte Mohamed DK, Veksha A, Ha QLM, Chan WP, Lim T, Lisak G. Advanced ni tar reforming catalysts resistant to syngas impurities: current knowledge, research gaps and future prospects. Fuel 2022;318:123602. https://doi.org/10.1016/j.fuel.2022.123602.
[58] Ohno T, He Z, Sleighter RL, Honeycutt CW, Hatcher PG. Ultrahigh resolution mass spectrometry and indicator species analysis to identify marker components of soil- and plant biomass-derived organic matter fractions. Environmental Science & Technology 2010;44(22):8594–600. https://doi.org/10.1021/es101089t.
[59] Hertzog J, Carré V, Le Brech Y, Dufour A, Aubriet F. Toward controlled ionization conditions for esi-ft-icr-ms analysis of bio-oils from lignocellulosic material. Energy & Fuels: An American Chemical Society Journal 2016;30(7):5729–39. https://doi.org/10.1021/acs.energyfuels.6b00655.
[60] Santamaria L, Lopez G, Arregi A, Amutio M, Artetxe M, Bilbao J, et al. Influence of the support on ni catalysts performance in the in-line steam reforming of biomass fast pyrolysis derived volatiles. Applied Catalysis. B, Environmental 2018;229:105–13. https://doi.org/10.1016/j.apcatb.2018.02.003.
[61] Santamaria L, Lopez G, Arregi A, Amutio M, Artetxe M, Bilbao J, et al. Stability of different ni supported catalysts in the in-line steam reforming of biomass fast pyrolysis volatiles. Applied Catalysis. B, Environmental 2019;242:109–20. https://doi.org/10.1016/j.apcatb.2018.09.081.